IEEE Access
Multidisciplinary | Rapid Review | Open Access Journal

Received March 4, 2019, accepted March 24, 2019, date of current version April 15, 2019.

Digital Object Identifier 10.1109/ACCESS.2019.2908018

Effective SNR Mapping and Link Adaptation Strategy for Next-Generation Underwater Acoustic Communications Networks: A Cross-Layer Approach

ISHTIAQ AHMAD[1,2] AND KYUNGHI CHANG[1], (Senior Member, IEEE)
[1]Department of Electronic Engineering, Inha University, Incheon 22212, South Korea
[2]Gomal University, Dera Ismail Khan 29050, Pakistan

Corresponding author: KyunhHi Chang (khchang@inha.ac.kr)

This work was supported by the project titled Development of Distributed Underwater Monitoring and Control Networks through the Ministry of Oceans and Fisheries, South Korea.

ABSTRACT Interest in the study of next-generation underwater sensor networks for ocean investigation has increased owing to developing concerns over its utilization in areas, such as oceanography, commercial operations in maritime areas, and military surveillance. The underwater base station controller, in the form of a surface buoy, communicates with underwater base stations (UBSs) while the UBSs transceiver information with underwater sensor nodes via acoustic communications. This paper provides a link-level and system-level study of downlinks using an orthogonal frequency-division multiple access techniques for underwater acoustic communications (UAC) networks. We present an approach to link-level-to-system-level (L2S) mapping at the link level that provides an abstraction model of the link-level performance to be accessed by system-level simulation (SLS). In this paper, an exponential effective signal-to-noise ratio (SNR) mapping (EESM) method is adopted, which elaborates on how multi-state channels are integrated into a single state in an SLS, and why an effective SNR can represent the characteristics of a multiple subcarrier SNR. Moreover, we explain the beta calibration procedure in detail for a UAC network. The simulation results are provided to verify the beta calibration of the UAC network. Furthermore, we employ a link adaptation strategy by evaluating system throughput based on a proportional fair (PF) scheduler at the system level. Hence, the simulation results confirm the effectiveness of link adaptation strategy for UAC networks.

INDEX TERMS UAC network, underwater channel model, L2S mapping, EESM, link adaptation.

I. INTRODUCTION

Next-generation underwater sensor networks have great potential for observing and exploring the aquatic environment. Therefore, underwater acoustic communications (UAC) is broadly considered to be the only approach feasible for long-distance underwater communications, and it has been extensively adopted in various scenarios. The demand for quality of service arises in many military, scientific, and civilian applications, including communications between submarines, for underwater security surveillance, for scientific data collection at ocean-bottom stations, in offshore oil explorations by autonomous underwater vehicles, and for data exchange in underwater sensor networks for environmental monitoring [1]. However, it is critical to deal with the underwater acoustic channel's challenging properties, such as long delay and large Doppler spread, resulting in frequency and time-selective fading. Moreover, fading, Doppler spread, and multipath propagation severely impact UAC network performance. Unlike typical wireless channels, the transmission loss in a UAC network not only depends on the distance between transmitter and receiver, but also on the signal frequency [2]–[5]. Absorption loss caused by the signal frequency is due to the transfer of acoustic energy

The associate editor coordinating the review of this manuscript and approving it for publication was Waleed Ejaz.

into heat. Hence, the underwater channel presents formidable challenges when comparing it with the typical terrestrial channel model.

Due to the extreme limitations on the available bandwidth in a UAC network, frequency reuse and cellular concepts are more appealing in order to enhance the coverage and capacity for a UAC network [6]–[8]. In this paper, we focus on the cellular type of UAC network architecture, in which the center cell is the region of interest and the first tier is just considered an interference-providing area. Indeed, assessment of the link-level simulation (LLS) has been measured by the SNR versus the block error rate (BLER) [9]. In order to achieve the BLER in the SLS without executing the actual computations, we utilize the BLER curves acquired by the LLS under an additive white Gaussian noise (AWGN) channel with respect to corresponding modulation and coding scheme (MCS) levels. An AWGN-equivalent signal-to-interference-plus-noise ratio (SINR) is needed in order to predict the BLER under a fading channel [10]–[13]. In this paper, we adopt the exponential effective SNR mapping (EESM) method for the L2S interface in the UAC network. We abstract the physical (PHY) layer by considering single-input, single-output (SISO) antenna configurations with the AWGN channel. The effect of fading channels or AWGN will be approximately the same after averaging the different SNRs by using the EESM method, and that is why we use an AWGN channel [14]. For clarity, this work determines the features of cross-layer, effective SNR mapping and a link adaptation strategy for next-generation UAC networks. The medium access control (MAC) layer handles the multiplexing of logical channels, and uplink and downlink scheduling, etc. The PHY layer controls coding/decoding, modulation/demodulation, multi-antenna mapping and further PHY layer functions. Link adaptation affects both MAC and radio link control (RLC) processing. The attachment of a cyclic redundancy check for error detection and correction, performing coding and modulation, and transmission of the resulting signal are all done by the PHY layer. The use of a cross-layer approach in a UAC network is based on the joint functionality of multiple layers. The information from the PHY layer is used at a higher layer in a cross-layer manner to execute link adaptation based on varying channel conditions. The channel quality indicator (CQI) manager at the PHY layer processes each received CQI report for scheduling decisions and for link adaptation purposes. The MAC layer contains the packet scheduler, but the exchange of information is performed at both higher and lower layers. For cross-layer optimization, we calibrate the beta value for three modulation schemes and find the optimal beta value for L2S mapping at the PHY layer, using this optimize parameter effect at the MAC layer for scheduling purposes in the UAC network.

A. MAIN CONTRIBUTIONS

The main contributions of this paper are as follows.

1) We adopt the general procedures for L2S mapping and link adaptation at the LLS and SLS, respectively, for a UAC network. To the best of the authors' knowledge, this work is the first to take care of L2S mapping issues at the LLS to abstract the PHY layer for development of a complete UAC SLS. In addition, our main concern is to point out the effectiveness of the link adaptation approach by considering the practical environment of underwater communications systems.
2) In the LLS, we focus mainly on the beta calibration procedure, using SNR-versus-BLER curves based on the EESM algorithm to find the beta values for the L2S interface of the UAC network. We perform beta calibration for three modulation schemes (binary phase-shift keying [BPSK], quadrature phase-shift keying [QPSK], and 16-phase quadrature amplitude modulation [16QAM]) for the UAC network. We take enough fading channel realizations to calibrate the beta values, and check the mean square error. The beta value that gives the minimum mean square error is selected as the optimal value.
3) In the SLS, we analyze the link adaptation strategy based on an adaptive modulation scheme under UAC network channel characteristics. We define important priority rules for choosing the MCS levels. Based on these priority rules, we select the final nine MCS levels for a link adaptation procedure in the UAC network.
4) Owing to the limitations of the available bandwidth, we utilize the concepts of frequency reuse and a cellular layout structure in order to increase the bandwidth efficiency of UAC network systems.

The rest of the paper is arranged as follows. In Section II, we discuss the prior works related to our topic. In Section III, we provide an explanation of a UAC network system model that contains a cell layout, and we provide UAC network channel model details. Section IV explains in detail the effective SNR approach to link-level-to-system-level mapping. Section V provides analysis of the link adaptation strategy in the UAC network SLS. Finally, conclusions are drawn in Section VI.

II. RELATED WORK

Plenty of work has been proposed in the literature to find features of UAC networks. This section briefly discusses the ample range of contributions related to them. Recently, UAC network researchers are paying considerable attention to scientific and commercial applications, environmental and pollution monitoring, assisted navigation, tactical surveillance, and disaster prevention [15]. For the feasibility of these applications, it is necessary to enable communications between underwater devices [16]. The standards have not yet been defined for several aspects related to UAC networks, such as PHY layer issues, transmission modes, protocols in the link, network, and transport layers [17]. In [18], the author presents the modeling of resources in virtual ocean environment. In [19], delay aware scheduling algorithm is proposed for underwater networks. In [20], the author compares the proposed orthogonal signal division technique with the conventional scheme for underwater networks. In this section, we

discuss the prominent approaches (frequency division multiple access (FDMA), carrier-sense multiple access (CSMA), code division multiple access (CDMA) and time division multiple access (TDMA) for the PHY and MAC layers. Due to the limitations on the available bandwidth in UAC channels and challenging properties such as long delay and large Doppler spread, the FDMA approach may not completely overcome the issues of UAC networks [21]. However, much of the research utilized the FDMA approach for special topologies and node deployment restrictions in UAC networks. In [22], the author introduces the OFDM-based MAC protocol for underwater sensor networks. In [23] the proposed MAC design exploits the multi-path characteristics of a fading acoustic channel. In the CSMA approach, the nodes sense the availability of the carrier in the channel before accessing it during the contention process. The carrier sensing cannot designate the actual status of the channel due to the long propagation delay of the acoustic signal. This may result in severe collisions. To overcome this issue, multiple access collision avoidance protocols were derived in which nodes lock the channel with previous request-to-send and clear-to-send messages. This, however, lessens the throughput [24]. In [25], the author examines that how multiple access collision avoidance protocol can be adapted for multi-hop UAC networks. In [26], proposed collision avoidance relieves the hidden terminal problem which is useful for UAC networks.

In the case of CDMA, a lot of research has been proposed to solve the near–far problem by controlling transmission power. The hierarchical tree topology was proposed in [27] in which nodes at the same hierarchical level are multiplexed by means of dissimilar orthogonal codes. In [28], the authors proposed diverse network sizes and architectures in order to relax the network topology restrictions. In [29], the authors compared the performance (energy consumption and throughput) of the slotted floor acquisition multiple access MAC and Tone-Lohi protocols.

In the literature, multiple TDMA-based protocols have been proposed to resolve the shortcomings of TDMA. In [30], the authors conducted real-time analysis of UAC networks. The routing policy selects the shortest path between the source and the sink node. They evaluated the performance of the proposed MAC protocol and routing model via simulations to address real-time communications in a UAC network.

In addition, a UAC network requires a multi-hop network to cover large areas. Numerous routing protocols have been proposed in the literature for UAC networks. The depth-based routing protocol was proposed in [31], which utilized the depth sensed by each node as a routing metric. In [32], an alternative dynamic routing protocol was proposed, which is related to hop count from the transmitter to the receiver node. In [33], the authors reviewed UAC network protocols for energy efficiency and reliability. They identified the pros and cons of different protocols based on different parameters, such as routing approach scalability, mobility, throughput, network topology, scheduling, contention, and acknowledgment schemes. In [34], the authors analyzed the throughput for a three-dimensional UAC network with a one-hop mobile relay. Dynamic UAC networks with mobile relays and static communications nodes were considered, and the packet delivery rate was chosen as a performance measure. A survey on routing protocols for UAC networks was provided in [35], where each protocol was presented based on routing strategy, merits, flaws, and latency. In [36], the authors proposed a mobility assisted geo-opportunistic routing paradigm to avoid interference in UAC networks. The mobile nodes directly collect the data from the void regions, and that minimizes the data traffic on intermediate nodes.

Moreover, from the view of capacity analysis, the analysis should be divided into LLS and SLS for UAC networks. In [37], the basic principles of wireless communication are described in detail with respect to LLS and SLS. Many researches have been proposed in terrestrial network such as power control between heterogeneous networks [38], analyzing the co-channel interference for overlapped networks [39], resource allocation [40], device discovery scheme with contention resolution [41]. So great concerns and practical researches on underwater networks are urgently required. Like terrestrial networks, author has considered the cellular-based network with tradeoffs between frequency reuse and user density [42]. Other researchers [43]–[49] addressed the PHY layer issues and network layer issues based on LLS and SLS analysis. In [44], an LLS capacity analysis of point-to-point links was provided. The theoretical bounds were derived between communication bandwidth and distance, as well as traversal capacity for a single link. This communications model can be expanded to the interference link [45], multiple antennas and relay networks [46]. Network-level capacity analyses have been provided [47], [48]. In [47], the authors evaluated the performance of a water-borne self-organizing network in the presence of interference. The nodes were deployed based on uniform distribution using the path loss and Lace fading. The simulation results illustrated that network connectivity is enhanced by selecting the appropriate frequency, transmission power, and bandwidth. In [48], throughput was analyzed based on network topology and the propagation environment. The authors considered a Poisson distribution for node deployment using a Rayleigh fading channel. In [49], a new architecture for UAC networks, called softwater, was introduced. The authors utilized the concept of software-defined networking for next-generation UAC systems.

Generally, a capacity analysis for existing UAC networks is mostly focused on static and deterministic networks. However, a capacity analysis for dynamic and random networks has not been fully studied in UAC networks. Hence, there is a dire need for further research into capacity analysis for UAC networks.

A. DIFFERENCES IN SYSTEM METHODOLOGIES IN THE LITERATURE

We highlight the major differences in the system methodologies of some important contributions. In [50], the authors

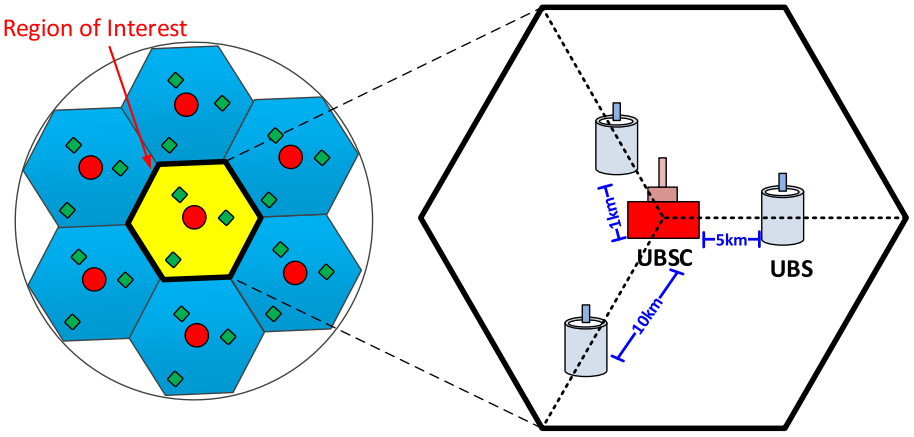

FIGURE 1. Cellular layout for the UAC network.

proposed a sweep–spread carrier method to improve SNR. The sweep is considered as a carrier signal that permits separate multipath arrivals by converting their time delays into a frequency reallocation. The major difference in this work is the sweep–spread technique for UAC networks, which is a totally different approach from our design, and the authors investigated only the feasibility of their own approach. In [51], the authors considered five discrete modulation and coding pairs with a finite number of transmission modes. An effective SNR is considered a working mode indicator, which is different from the input SNR and pilot SNR. The major difference in this work is using the different sizes of MCS levels in the system. In [52], the authors designed a chirp-based feedback channel and an adaptation mechanism of real-time PHY layer communications parameters, or seamless switching between different technologies, such as orthogonal frequency division multiplexing and direct sequence spread spectrum. Different philosophies and targets of system designs by other researchers [50]–[52] resulted in totally different system parameters.

III. UAC NETWORK SYSTEM MODEL

There are many contributions of cellular-based network topologies, as well as frequency reuse concepts in terrestrial networks [37]–[41]. The tremendous achievements of cellular networks are enough motivation to consider the cellular and frequency reuse concept in a UAC system. The UAC network is still in the development stages, and that is why a lot of attention and meaningful research is required in this area. Because of bandwidth limitations, the cellular-based network structure for a UAC network is appealing [42]. In this paper, we emphasize the downlink cellular type of network structure for a UAC network.

A. STRUCTURE FOR THE UAC NETWORK

The network layout is based on the basic cellular concept of spatial frequency reuse. Fig. 1 shows the considered architecture of a one-tier UAC network layout. The red circles represent the underwater base station controller, or buoy, while the green squares show the UBSs. The inter-site distance between the underwater base station controllers is 40 km, and three UBSs are connected to one underwater base station controller. The yellow region represents the region of interest. It means that the central cell is the region of interest in which three UBSs are connected to the underwater base station controller via acoustic communications link 1 (underwater base station controller to UBS) with fixed distances, i.e., short (1 km), medium (5 km), and long (10 km). The term region of interest means that the scheduling, outage, and throughput calculation, etc., will be done only for the users exist in the region of interest. The region of interest varies based on the scenarios assumed by the authors. In our 1-teir UAC network scenario, we assumed that the center cell is our region of interest. as described by the yellow color in the Fig. 1. The blue area is the interference-providing area, i.e., we do not consider the UBSs in first tier.

B. UAC NETWORK CHANNEL MODEL

The UAC network channel model has severe effects on system performance due to its challenging characteristics. So, it is important to consider transmission loss, ambient noise, and multipath fading effects when analyzing the link adaptation in the SLS to increase the bandwidth efficiency of the UAC network [43].

Indeed, the main purpose for consideration of the cellular type of architecture under the UAC network channel model is to maximize the coverage and capacity within limited bandwidth resources. The main difference between the terrestrial network and underwater network is considering the underwater channel model. However, equations (1) - (8) and their corresponding figures are well known in the literature. We utilized these equations to verify the underwater channel model parameters for our system. So, it is necessary to keep that information (i.e., equation (1) – (8) and corresponding figures) for the credibility of our system model.

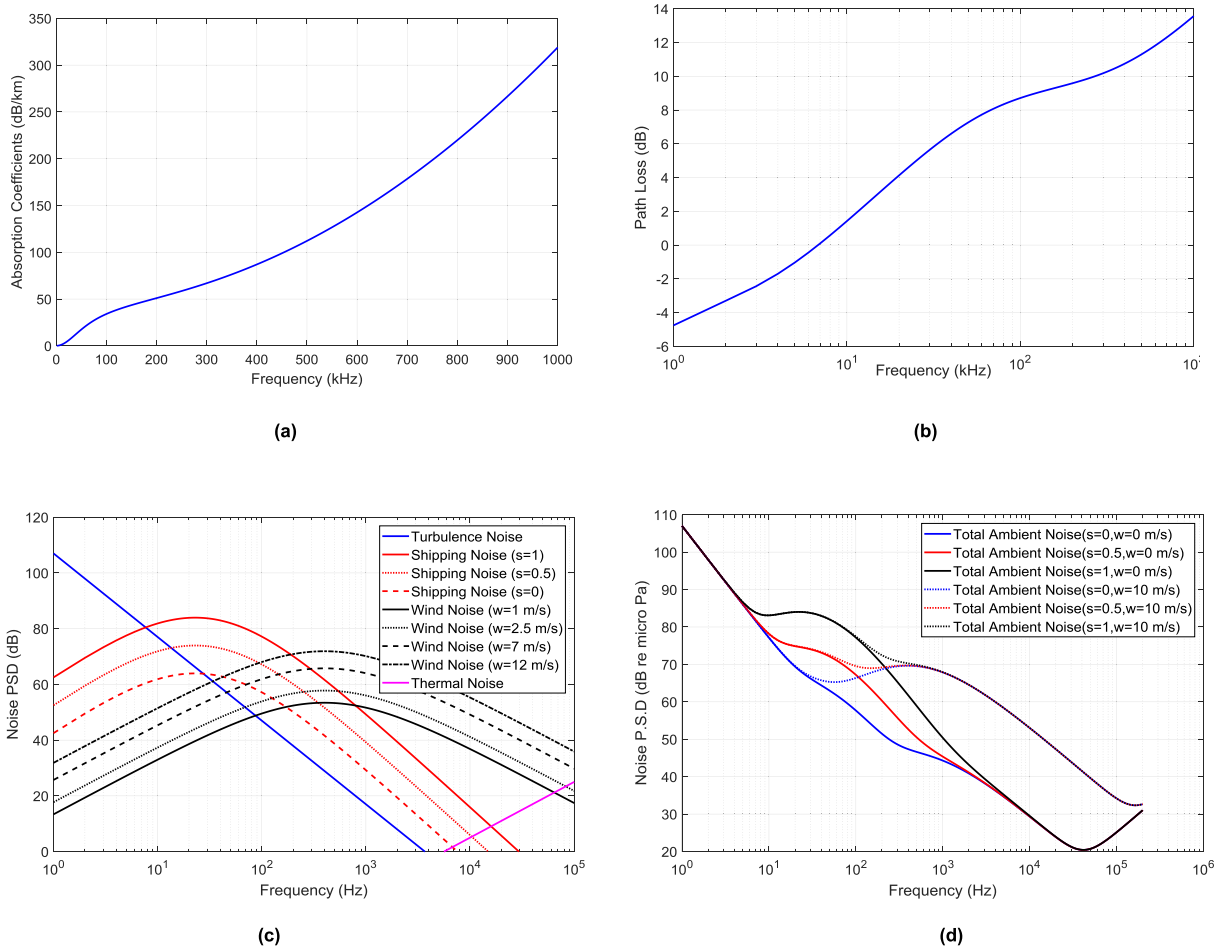

FIGURE 2. **(a) Absorption coefficient curve (b) Pathloss curve (c) Individual turbulence noise, shipping noise, wind noise, and thermal noise curves (d) Total ambient noise curves with varying shipping and wind factors.**

1) TRANSMISSION LOSS

In a UAC network, transmission loss is due to geometric spreading loss and attenuation. We choose the most representative transmission loss model that was used in a lot of previous research [43], [44], [53]. It can be represented as follows:

$$A(d_i, f) = A_0 d^k \alpha(f)^t \tag{1}$$

where A_0, k, and $\alpha(f)$, respectively, are a unit normalizing constant, the spreading factor, and the absorption coefficient. The expression of the transmission loss in decibels can be written as:

$$10 \log\ A(d,f)/A_0 = k.10 \log\ d + d.10 \log\ \alpha(f) \tag{2}$$

In (2), the first term represents the spreading loss (the value of the practical spreading factor is k = 1.5), and the second part denotes the absorption loss. The absorption coefficient is due to the signal frequency and can be represented empirically using Thorp's formula [3], which expresses $\alpha(f)$ [dB/m] as a function of f [kHz]:

$$\alpha(f) = \frac{0.11 f^2}{1+f^2} + \frac{44 f^2}{1400+f^2} + 2.75 \times 10^{-4} f^2 + 0.003 \tag{3}$$

Fig. 2(a) and 2(b) show the absorption coefficient loss and complete transmission loss or path loss, respectively. The absorption loss and transmission loss are increased with the frequency.

2) AMBIENT NOISE

Ambient noise is natural in the UAC network channel model. The empirical formulae of major noise sources with their power spectral densities can be represented as follows [44], [53]:

$$\begin{aligned}
10 \log N_t(f) &= 17 - 30 \log f, \\
10 \log N_s(f) &= 40 + 20(s-5) + 26 \log f - 60 \log\ (f+0.03), \\
10 \log N_w(f) &= 50 + 7.5 w^{1/2} + 20 \log f - 40 \log\ (f+0.4), \\
10 \log N_{th}(f) &= -15 + 20 \log f,
\end{aligned} \tag{4}$$

where N_t, N_s, N_w, N_{th} stand for turbulence, shipping, wind, and thermal noise, respectively. The total noise power density

TABLE 1. Fading channel model parameters.

Tap	Delay Profile (ms)	Amplitude (dB)	K (dB)
1	0	0.0	43.50
2	0.06	0.39	52.48
3	1.51	-1.01	19.89
4	1.57	-3.09	119.11
5	1.68	-2.92	61.78
6	6.34	-4.69	12.56
7	6.38	-8.79	78.64
8	6.63	-9.46	31.74
9	6.68	-12.47	50.22
10	14.38	-14.23	50.53
11	14.51	-19.46	31.64
12	17.78	-18.98	12.59

is represented as:

$$N(f) = N_t(f) + N_s(f) + N_w(f) + N_{th}(f). \tag{5}$$

Fig. 2(c) shows the four kinds of ambient noise (turbulence, shipping, wind, and thermal) individually. In shipping noise, s is the shipping activity factor, which ranges between 0 and 1 for low and high activity, respectively. For wind noise, w represents the wind speed in meters per second, which comes from the surface motion caused by wind-driven waves. Hence, the total ambient noise is the summation of the overall power spectral densities of turbulence, shipping, wind, and thermal noise, as shown in Fig. 2(d).

3) TWELVE-PATH RICIAN FADING CHANNEL MODEL

We built Matlab-based LLS and SLS platforms, and utilized the 12-path Rician fading channel for UAC networks. The fading channel employed in this paper has 12 path delays, and every path has a different delay profile and K value. This fading channel model is based on one of the measured channels in the Korean sea, for which the channel model parameters are listed in Table 1. Moreover, the values for Doppler spread and maximum delay are 4 Hz and 17.78 ms, respectively. In addition, the numbers for maximum excess delay, coherence bandwidth, and coherence time are 14.78 ms, 16 Hz, and 250 ms, respectively. It should be noted that the data acquisition experiment is only conducted for the fading channel model. We use this data of the fading channel model in our simulations. The details of the experimental environment for the data acquisition of the fading channel are given as follows.

1) We conducted the experiment for data acquisition from Dec. 9, 2017, to Dec. 13, 2017.
2) The experiment was conducted in Korean sea (Pohang Sea, Geoje City, South Gyeongsang province).
   - The latitude and longitude coordinates were: 34° 49′ 59.13 N, 128° 45′ 13.83 E.

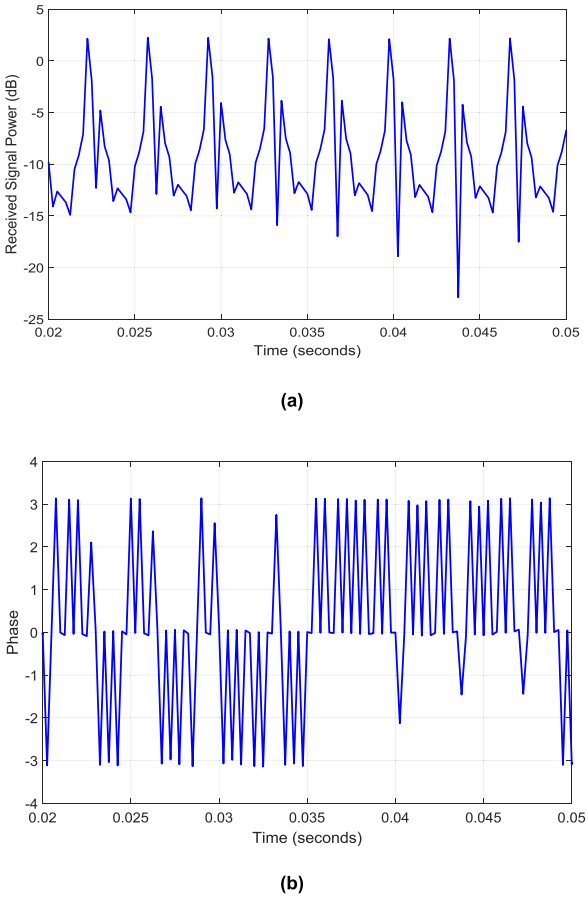

FIGURE 3. (a) Envelope generated by the 12-path Rician fading model. (b) Phase generated by the 12-path Rician fading model.

3) For the experimental setup, we set the depths of the transmitter (transducer) and receiver (hydrophone) to be 25 m and 5 m, respectively. We conducted the experiment based on different distances between transmitter and receiver, i.e., 500 m, 1 km, 1.5 km, 2 km, 5 km, and 10 km.
4) For the channel measurements, we considered the frequency range from 10 kHz to 14 kHz, with linear frequency modulated (LFM) and Zadoff-Chu signals used, and a signal bandwidth of 4 kHz.
5) The transmitting side periodically transmitted a signal, and the receiving side received the signal and estimated the impulse response of the channel. The channel was measured by varying the distance between the transmitting side and the receiving side.

The root mean square (rms) delay spread can be calculated as:

$$\sigma_\tau = \sqrt{\overline{\tau^2} - (\bar{\tau})^2} \tag{6}$$

where, $\bar{\tau}$ represents the mean excess delay.

In Fig. 3(a) and Fig. 3(b), we provide the fading envelope and phase of the 12-path fading channel model, respectively.

IV. EFFECTIVE SNR APPROACH FOR LINK-LEVEL TO SYSTEM-LEVEL MAPPING FOR UAC NETWORK SYSTEMS

Dealing with the receiver structure, coding schemes or feedback issues are suitable for simulation at the link level, but it is impractical to consider cell planning, scheduling, or interference issues in this type of simulation. However, it is not feasible in execution of system-level simulations to consider all the issues between the underwater base station controller and UBS links, because it requires massive amounts of computational power. Therefore, in order to decrease the complexity of the problem, we abstract the physical layer in the SLS by capturing the fundamental characteristics with high accuracy. Then, it is easy to analyze the performance of the whole network on the SLS side. In this paper, abstraction of the physical layer is done by using the EESM algorithm in the UAC network system.

In the L2S mapping procedure, the PHY layer input data are compressed into single values, typically called effective SNR (SNR_{eff}). The AWGN-equivalent SNR is attained with the EESM method, and is mapped to the BLER through AWGN link performance curves. Moreover, calibration and optimization of the beta scaling factor provides a more accurate L2S interface model.

A. BETA CALIBRATION PROCEDURE

For accurate L2S mapping, a beta adjusting factor is required in a UAC system. However, numerous simulations are needed for distinct channel realizations and to determine the beta adjusting factor that provides the least difference between the estimated BLER and the actual BLER [54]. In particular, SNR_{eff} points should be equivalent to the AWGN curve of the respective MCS. In this paper, we find the beta values for L2S mapping using the EESM approach. We use the UAC network twelve-path Rician fading channel model in order to obtain the different channel realizations.

A total of 10 channel realizations are simulated under the 12-path Rician fading channel model for the same MCS using the UAC network LLS. The detailed steps for the beta calibration procedure are as follows.

Step 1] Calculate the SNR values experienced by data subcarriers of the packets on the receiver side $[\text{SNR}_1, \ldots, \text{SNR}_n]$. All the SNR values belonging to a particular packet are compressed into a single scalar value.

Step 2] Calculate SNR_{eff} as follows [14]:

$$SNR_{eff} = -\beta \ln\left(\frac{1}{N}\sum_{i=1}^{N}\exp(-\frac{SNR_{N_i}}{\beta})\right) \tag{7}$$

To compare the two values gained from SNR_{eff} and SNR_{AWGN}, find the best possible beta value that minimizes the difference between the computed and actual effective SNR:

$$\beta = \arg\min_{\beta} \left\| SNR_{AWGN} - SNR_{eff}(\beta) \right\| \tag{8}$$

Algorithm 1 Implementing the Beta Calibration Procedure

Initialization

1. Set the number of Nc fading channel realizations $\mathbf{H}_n$.
2. SNR vector length n_s : $[\text{SNR}_1 \ldots \text{SNR}_{n_s}]$.
3. Gaussian noise variances $[\sigma_1^2 \ldots \sigma_{n_s}^2]$
4. Set a calibration vector $\beta = [\beta_1 \ \ldots \beta_l \ldots \beta_{n_b}]$

Generate the BLER values $C = \{\text{BLER}(\mathbf{H}_n, \sigma_k^2)\}_{n,k}$

- BLER $(\mathbf{H}_n, \sigma_k^2)$ is the BLER (over noise) for a given fading channel realization and noise variance.

for i = 1 to $N_{c=10}$ (for all channel realizations) **do**
  Generate channel $\mathbf{H}_n$
  for k = 1 to n_s (for all SNR) **do**
    for m = 1 to $N_{w=2000}$ (for 2000 iterations) **do**
      Generate additive noise w_m
      Calculate BLER $(\mathbf{H}_n, \text{w}_m)$
    end
    Calculate and save average (over noise) BLER:
    BLER $(\mathbf{H}_n, \sigma_k^2) = \frac{1}{N_w}\sum_{m=1}^{N_w}$ bler $(\mathbf{H}_n, \mathbf{w}_m)$
  end
end

Calibration Step

- Calculate effective SNR, $\text{SNR}_{eff}(\mathbf{H}_n, \sigma_k^2, \beta_l)$, according to (7) for each channel realization, noise variance, and calibration factor.
- Optimal calibration factor is:

$$\beta_{opt} = \arg\min_{\beta} \left\| SNR_{AWGN} - SNR_{eff}(\beta) \right\|$$

where

$$SNR_{AWGN} = [SNR_{AWGN,1}, SNR_{AWGN,2}, \ldots, SNR_{AWGN,n}] \tag{9}$$

$$SNR_{eff}(\beta) = [SNR_{eff,1}(\beta), SNR_{eff,2}(\beta), \ldots, SNR_{eff,n}(\beta)] \tag{10}$$

The equations (9) and (10) are representing the vectors with elements corresponding to the channel realizations.

Step 3] Many random channel realizations are required; then, calibrate the beta values to minimize the mean square error. The beta value that gives the minimum difference is selected as the optimal value.

Step 4] Map SNR_{eff} to the packet error rate (PER) or the BLER by using the AWGN-PER look-up table corresponding to the given MCS. Algorithm 1 shows the implementation details of the beta calibration procedure on the LLS side of the UAC network.

According to Algorithm 1, it is easy to understand the process of beta calibration. Primarily, we need to calculate the BLER curves under the AWGN channel model at the assumed MCS level. Next, multiple channel realizations are required under the specific channel model, and in this paper, we simulate attaining the different channel realizations under the 12-path Rician fading channel model. Then, we calculate the SNR values of the existing subcarriers for each channel realization. After that, SNR_{eff} or SNR_{eesm} values are

computed using EESM channel realization. Finally, we calculate the difference between SNR_{AWGN} and SNR_{eff} for the corresponding BLER. After all that, the process needs repetition for diverse beta values in order to achieve the minimum difference. In this paper, the EESM method of L2S mapping is summarized for a UAC network that provides EESM beta calibration for the three modulation schemes: BPSK, QPSK, and 16QAM over a 12-path Rician fading channel. We summarize the implementation steps of the beta calibration procedure in Algorithm I for the UAC network.

It should be noted that Algorithm I presents the implementation steps of beta calibration. We set the values of specific parameters to perform the beta calibration, such as the number of fading channel realizations (10), etc. It presents more precise implementation steps for the generic scenario. Our intention is to provide clear details, so readers understand the beta calibration procedure in the UAC network.

B. SIMULATION RESULTS FOR BETA CALIBRATION

In this paper, we find the beta values for the three modulation schemes (BPSK, QPSK, and 16QAM) using the EESM approach for a UAC network. The calibrated beta values are utilized to achieve accurate L2S mapping in the UAC network. In Fig. 4(a), we draw the actual curves for BPSK, while Fig. 4(b) shows the calibrated EESM curves. In Fig. 4(b), scattered markers represent the distinct channel realizations, which are dispersed near the AWGN curve (solid line). This demonstrates the validity of the abstraction model, because the estimated BLER is very close to the simulated BLER under AWGN. Similarly, Fig. 5(a), shows the actual curves for QPSK, while Fig. 5(b) presents the calibrated EESM curves. In Fig. 6(a), we draw the actual curves for 16QAM, while Fig. 6(b) shows the calibrated EESM curves. Hence, the scattered markers denote the BLER acquired over the 12-path Rician channel model, while the solid line represents the reference SNR-versus-BLER curve under AWGN, as shown in figures 4(b), 5(b), and 6(b).

The increment in variance at high SNR ranges is due to the fading channel realizations. From the figures (4), (4), and (6), the BLER curves of the fading channel realizations are overlapped at low SNR but these curves are little spread at high SNR due to high BLER. The increased variance of the effective SNR is imitating the fading channel realization. Hence, the variance of the effective SNR is low at low BLER and vice versa.

Moreover, the reason for taking the 10 realizations of the fading channel model is quite obvious. From the figures (4), (4), and (6), it can be easily observed that the curves of Rician fading channel are overlapping with each other. It means that 10 fading channel realizations are enough in our UAC system for link-level to system-level mapping.

V. ANALYSIS OF THE PROPOSED LINK ADAPTATION STRATEGY IN UAC NETWORK SLS

In this paper, we adopt the link adaptation strategy based on adaptive modulation schemes for a UAC network. Typically,

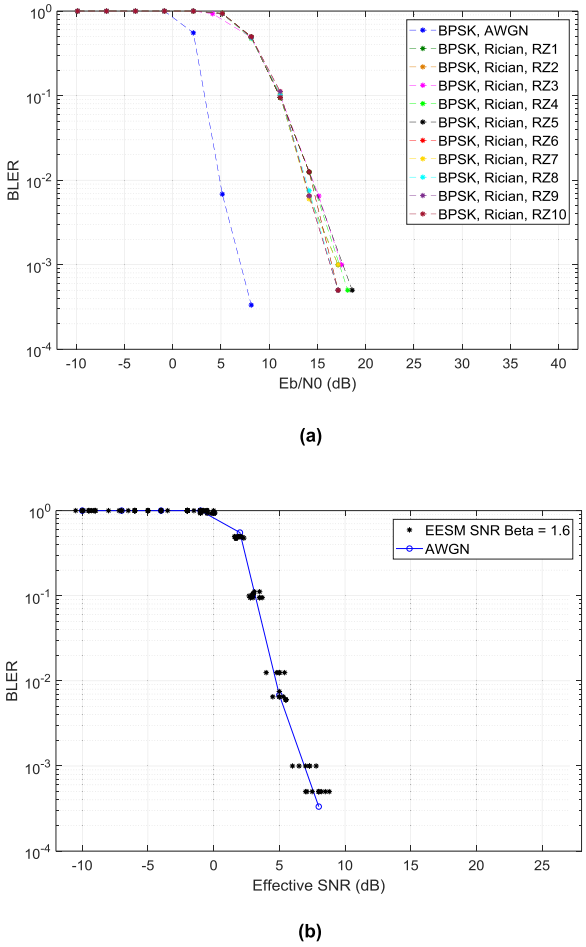

FIGURE 4. EESM beta calibration for BPSK over a 12-path Rician fading channel in a UAC network: (a) BPSK curves, and (b) calibrated curves.

a high SNR imitates the higher order modulation scheme, which provides high spectral efficiency. In contrast, a low SNR follows the lower order modulation scheme; although it provides less spectral efficiency, it is robust against transmission errors. In this paper, we consider BPSK, QPSK, and 16QAM modulation schemes with a constant code rate (1/2) in the link adaptation strategy. Indeed, the data repetition patterns (RPs) corresponding to each modulation scheme are considered. There are some important data RPs (1, 3, 4, 8, 9, 12, 24, 36, 72) considered on the LLS side. So, a total of 27 MCS levels exist, based on the combination of the three modulation schemes and RPs, which are shown in Fig. 7. However, there is overlap between the different MCS levels, and hence, we assume some important priority rules for selecting the MCS levels from Fig. 7, as follows.

- Select MCS levels with at least a 1 dB difference from each other.
- If the different MSC levels (BPSK, QPSK, 16QAM) have less than a 1 dB difference between them, then select the MCS that has a better BLER.
- In case of overlap between the different MSC levels, select the lower MCS.

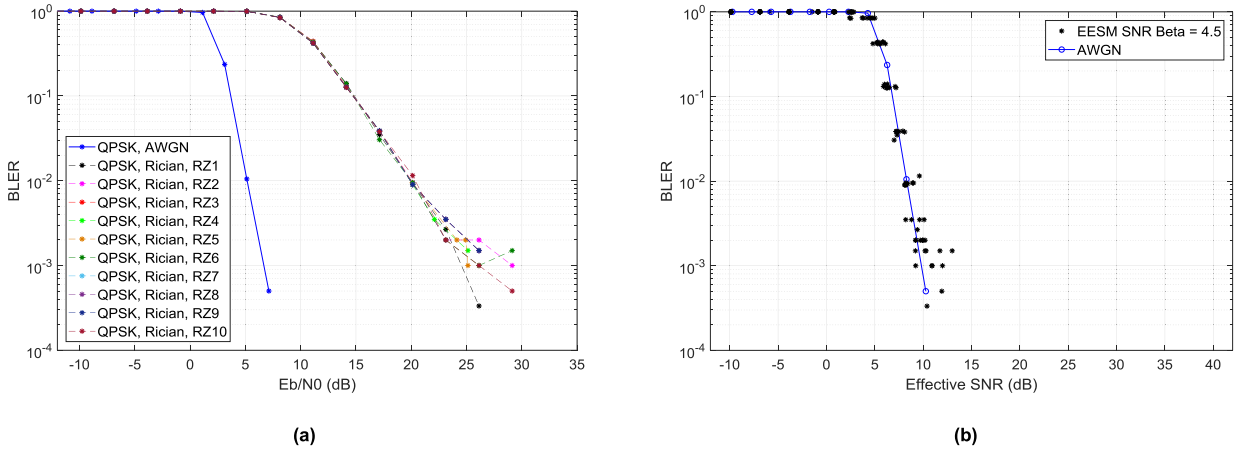

FIGURE 5. EESM beta calibration for QPSK over a 12-path Rician fading channel in a UAC network: (a) QPSK curves, and (b) calibrated curves.

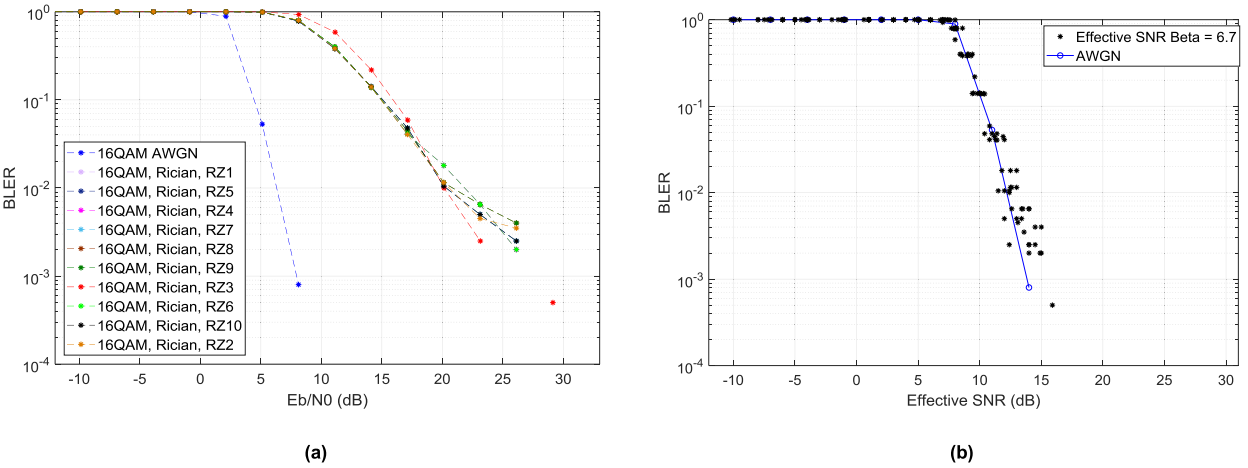

FIGURE 6. EESM beta calibration for 16QAM over a 12-path Rician fading channel in a UAC network: (a) 16QAM curves, and (b) calibrated curves.

- If the same MCS levels have different RPs (e.g., BPSK RP1, BPSK RP3) and they also have less than a 1 dB difference between them, then select the MCS that has the better BLER.
- If different MCS levels have different RPs but a very small difference in the BLER, then select the lower MCS.
- Discard the lower MCSs with greater RPs in low SNR ranges, because that has no impact on system throughput (e.g., BPSK RP72, BPSK RP36, BPSK RP24, QPSK RP72, etc.).
- Keep the MCS levels that have a lower RP pattern, because that has a significant impact on system throughput (e.g., BPSK RP1, QPSKRP3, 16QAM RP3).

The discarded MCS levels based on the priority rules are shown in Fig. 8. So, 13 MCSs remain by applying the priority rules for the selection of MCS levels from among the 27 MCS levels. Now, we utilize the remaining 13 MCS levels in the SLS to analyze the system throughput at each MCS level. Fig. 9 shows throughput curves based on the remaining 13 MCS levels. From Fig. 9, it is easy to see that we need to discard the high-order MCS levels because they overlap with low-order MCS levels (e.g., QPSK RP12 overlaps BPSK RP3). Hence, we discard four more MCS levels (BPSK RP8, QPSK RP12, QPSK RP4, and 16QAM RP12) based on the SLS throughput curves. After discarding those four MCS levels, the BLER curves of the finalized MCS levels are shown in Fig. 10. Moreover, the SNR-versus-CQI mapping based on the final nine MCS levels for adaptive modulation in the UAC network SLS is shown in Table 2.

We utilize the finalized nine MCS levels in our link adaptation strategy by evaluating throughput in the UAC network SLS using PF scheduling in the frequency domain. Moreover, we consider link adaptation in the frequency domain, while in the time domain, we perform scheduling based on round robin (RR) UBS selection and PF UBS selection. In the RR-based UBS selection strategy, we allocate one frame to one UBS in each time slot based on the RR UBS selection, while link adaptation is performed in the frequency domain for the corresponding UBS time slot. For the PF-based

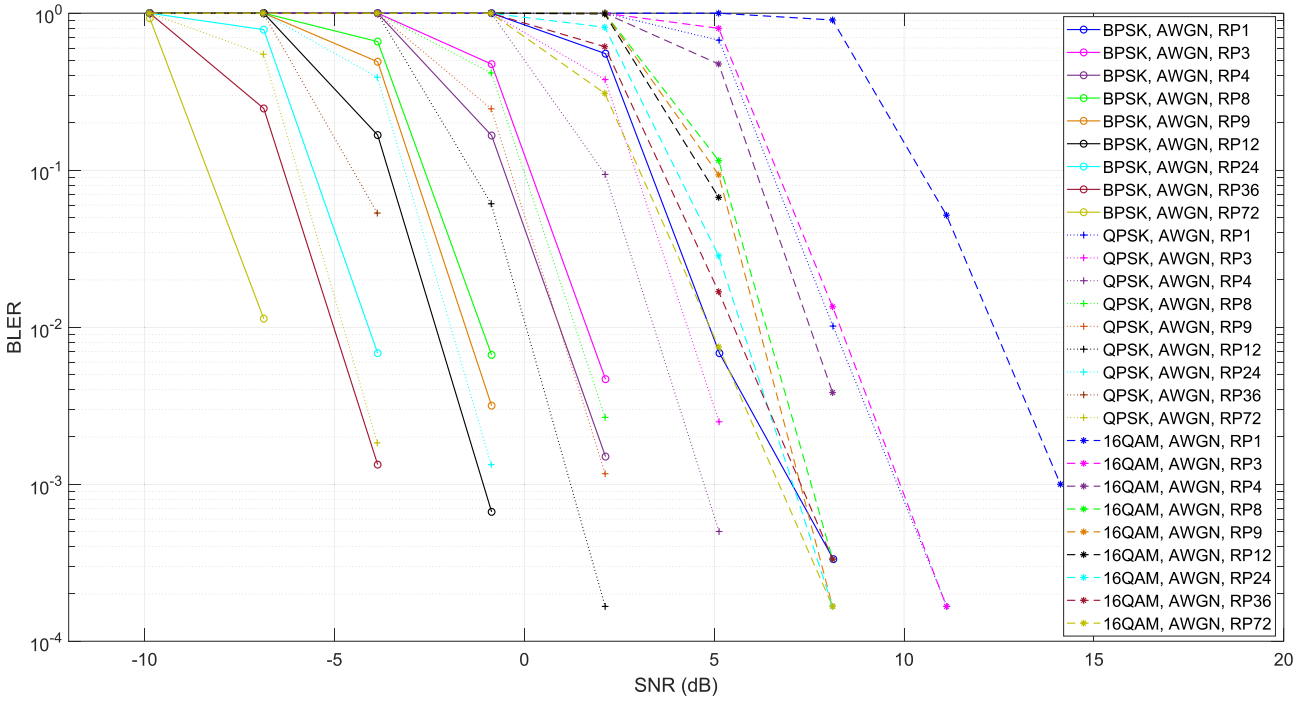

FIGURE 7. MCS levels based on the combination of three modulation schemes and RPs.

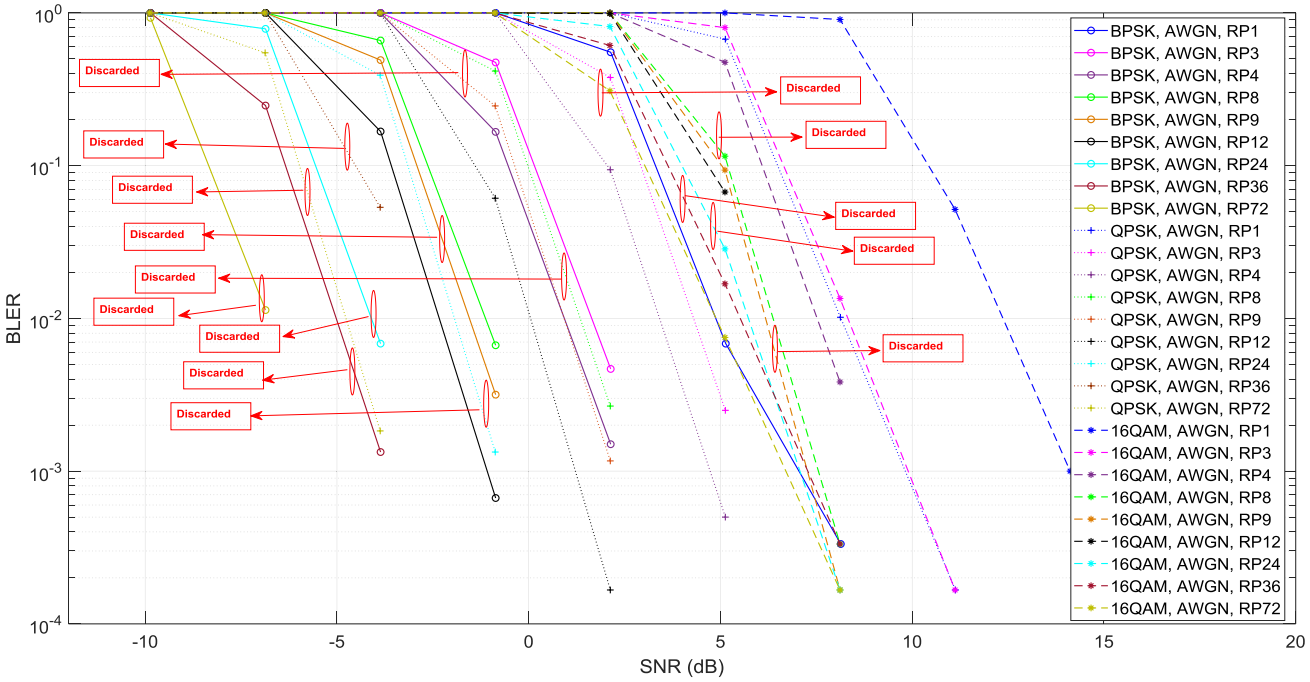

FIGURE 8. Discarded MCS levels based on the priority rules for selecting the MCS levels.

UBS selection strategy, we allocate one frame in each slot to the UBSs based on the PF UBS selection, while link adaptation is also performed in the frequency domain for the corresponding UBS time slot. Fig. 11 (a) and (b) show the details of time domain scheduling for RR-based UBS selection and PF-based UBS selection, respectively.

The implementation details of the link adaptation procedure for adaptive modulation based on the finalized nine MCS levels in the UAC network SLS is shown in Algorithm II.

Algorithm 2 Implementation of Link Adaptation Procedure

Initialization
Initialize $x \leftarrow 1, x_{\max}$ **do**
$CP = 1/4, FFTSize = 512, SISO, PS = 2, CQIs = 9,$
$MCS\_levles = 9 \leftarrow (TotalRPs : 9, CR : 1/2)$
Step 1 SNR Thresholds for MCS Levels
- Assign the SNR Threshold for different MCS levels based on SNR vs. BLER curves by using the 10% BLER values of each curve.

$CQI\_index : MCS\_levels$
for each CQI_index
Assing *SNRThreshold*
end
Step 2 UWN Channel Characteristics Effects
- Channel Characteristics: Delay Spread, Doppler Spread, Large-scale effects, Small-scale effects
- Calculate the received SNR after passing the channel and send CQI feedback on each RB to the transmitter.

Apply *Channel*
for each *RB*
Calculate *Rx_SNR*
for
Assing $CQI\_index \leftarrow Rx\_SNR$
end
Send *CQI_feedback*
end
Step 3 Determine MCS Level
- Determine MCS level of each RB by comparing the received SNR with thresholds SNRs for different MCS levels.

for $x \leftarrow 1, x_{\max}$ **do**
Compare $(CQI\_feedback, SNRThreshold)$
Select MCS_level
end
Step 4 Resource Scheduling
- Based on the selected MCS level transmitter performs resource scheduling.

for each MCS_Level
do Resource Schduling
end

Note that the process of adaptive modulation is based on the frequency domain while allocating a frame in each time slot. Consequently, scheduling is done in the frequency domain based on PF rules for adaptive modulation in the UAC system. The implementation steps of the link adaptation procedure are described in Algorithm II.

A. COMPUTATIONAL COMPLEXITY OF THE LINK ADAPTATION PROCEDURE

The computational complexity is measured by considering the elementary operations required for the procedure to run, and denote as a function of the problem size, K (the total number of resource blocks). The complexity of the water-filling adaptive modulation and coding model in [55], represented by $T(K)$ operations, is specified as:

$$T(K) = O(M * \zeta(2K + 2S_{EF} * K + S_{ET} * K)) \quad (11)$$

where M represents the multiple-input, multiple-output (MIMO) transmission modes, ζ is the number of coding rates, K is the total number of resource blocks or subcarriers, and S_{EF} and S_{ET} represent the number of iterative searches to

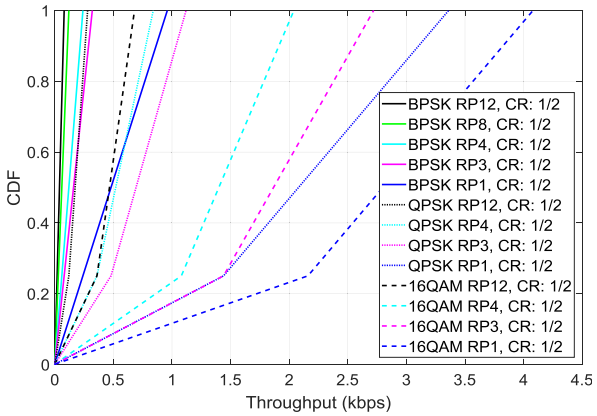

FIGURE 9. Throughput curves (13 MCS levels).

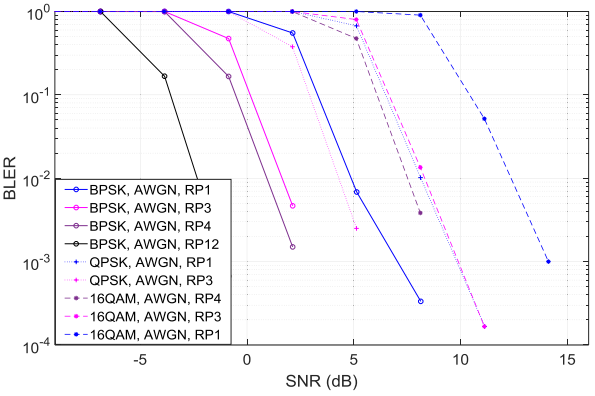

FIGURE 10. Final MCS levels.

TABLE 2. CQI table for MCS levels of adaptive modulation in a UAC network SLS.

CQI	Modulations with Repetition Patterns	Code Rate	SNR (dB)
1	BPSK, RP12	1/2	-3.6
2	BPSK, RP4	1/2	-0.6
3	BPSK, RP3	1/2	0.1
4	QPSK, RP3	1/2	2.9
5	BPSK, RP1	1/2	3.4
6	16QAM, RP4	1/2	6.1
7	QPSK, RP1	1/2	6.9
8	16QAM, RP3	1/2	7.2
9	16QAM, RP1	1/2	10.4

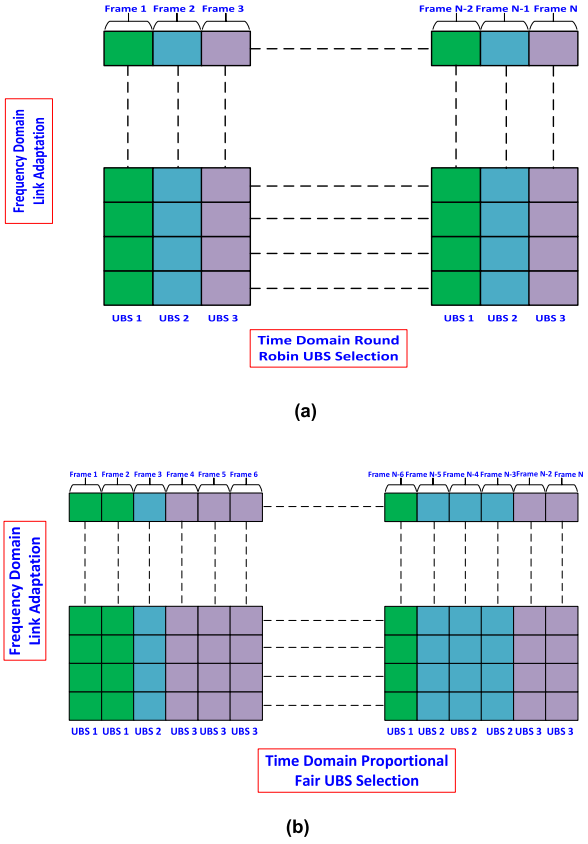

FIGURE 11. Example scheduling for UAC network (a) Time domain RR-based UBS selection (b) Time domain PF-based UBS selection.

acquire the solutions for the efficiency and E-tightening subroutines, respectively. In the worst-case scenario, these two parameters (S_{EF} and S_{ET}) may increase to K, as determined by the initial bit allocation in [56].

For the block adaptative modulation and coding model in [57], the complexity is described as follows:

$$T(K) = O(M^{*}L * K) \tag{12}$$

where L denotes the MCS level ($L = 1, \ldots, L_{\max}$). The dependence of (12) on the resource blocks or subcarriers comes from computation of the instantaneous Bhattacharyya factor in the bit error probability estimation. The computational complexity of the link adaptation strategy adopted in this paper for the UAC network is described as follows:

$$T(K) = O(M^{*}K * P) \tag{13}$$

where P represents the number of repetition patterns ($P = 1, \ldots, P_{\max}$), K is the total number of resource blocks, and M represents the MIMO transmission modes regarding space and time. In our case, we utilize a single antenna at the transmitter and a single antenna at the receiver. Since, the complexity of our approach is low, battery drain would not be an issue. Hence, the terms in (13) represent the serial selection of MCS levels followed by link adaptation.

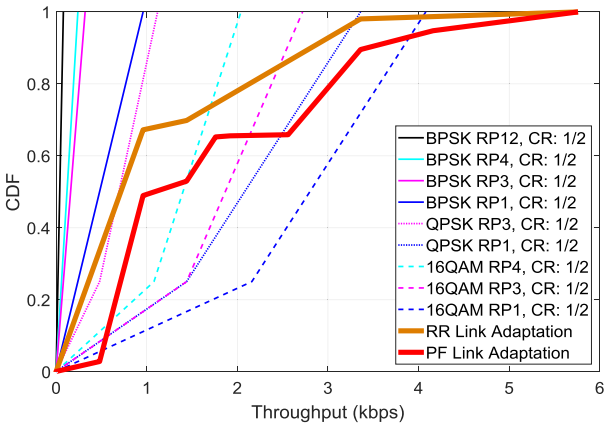

FIGURE 12. Resulting throughput curves of each MCS level from the link adaptation strategy.

Fig. 12 gives the UAC network SLS throughput based on individual MCS levels and link adaptation curves. We can easily see that the bold red and brown curves imitate the adaptive modulation strategy based on the finalized nine MCS levels. Hence, the bold red and brown curves show the effectiveness of link adaptation in the UAC network SLS based on PF and RR UBS selection, respectively. Link adaptation with PF UBS selection has better performance than link adaptation with RR UBS selection because it serves the UBSs fairly.

VI. SYSTEM-LEVEL SIMULATION RESULTS FOR PERFORMANCE EVALUATION OF PROPOSED LINK ADAPTATION STRATEGY

In this section, we employ the conventional adaptive algorithm [58] in our system to compare with our proposed link adaptation approach. The main objective of the adaptive algorithm in [58] is to maximize the throughput by allocating the highest modulation on each subcarrier when the targeted BER value does not exceed on that subcarrier.

A. SIMULATION ENVIRONMENT AND ASSUMPTIONS

To verify the analysis of proposed link adaptation strategy, system-level simulations are performed under 1-tier UAC network, as illustrated in Fig. 1. Our main concern is to prove that proposed link adaptation approach is working efficiently in the UAC system with less computational complexity. From the Fig. 7, it can be easily observed that there are irregularities between the MCS levels which degrades the system performance if the link adaptation approach is applied directly. The main objective of our proposed methodology is to reduce the irregularities between the MCS levels which results in less complexity and system will work efficiently while adapting the useful MCS levels for the UAC network. The priority rules are defined in section V.

In order to see the effectiveness of the proposed link adaptation strategy, we compare it with the conventional adaptive technique in [58]. So, we need to employ the conventional link adaptation technique in our designed system. The simulation environment is considered exactly same for conventional

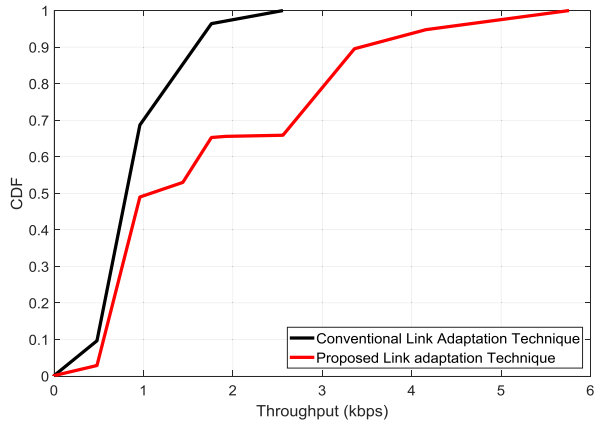

(a)

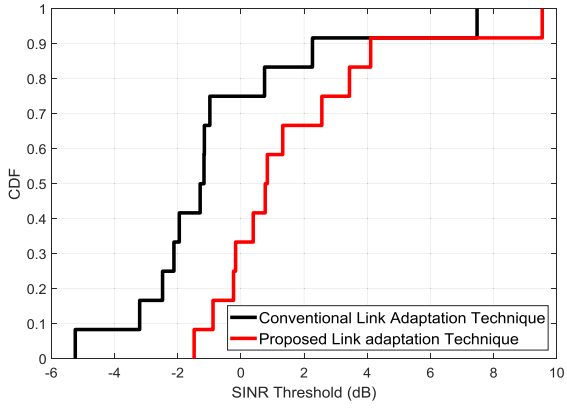

(b)

FIGURE 13. Performance comparison between the conventional link adaptation technique and the proposed link adaptation technique. (a) Throughput performance curves, (b) Outage probability performance curves.

link adaptation technique as we adopted for the proposed one. The main simulation parameters are described in the Table 3.

B. SIMULATION RESULTS AND DISCUSSION

This subsection compares the simulation results of the conventional link adaptation technique with the proposed one. The performance of the proposed link adaptation strategy is assessed using the important performance metrics such as throughput and outage probability.

1) THROUGHPUT PERFORMANCE CURVES

The throughput equation is:

$$Throughput = \frac{TB}{Accounted\_TTIs * TTI\_Time} \text{Kbps} \quad (14)$$

where TB is total bits for receiver j and accounted transmission time intervals (TTIs) are the maximum number of TTIs in which RBs assigned to receiver j. Fig. 13(a) shows the throughput performance comparison between the conventional link adaptation technique and proposed link adaptation technique. In Fig. 13(a), we calculate the throughput by using the (14) for the proposed and conventional link adaptation techniques. The throughput curves are not smooth due to less throughput resolution points in Fig. 13(a), because the receivers are achieving the throughput on same values. At the 50 % CDF, it can be clearly seen from the Fig. 13 that the throughput of the proposed link adaptation technique is around 1.1 kbps, but the conventional link adaptation algorithm could only achieve the throughput around 0.86 kbps. Hence, the proposed link adaptation technique outperformed around 24.5 % than the conventional one. The reason for achieving the higher throughput by the proposed link adaptation strategy is quite-obvious, i.e., system is adapting the links smoothly with less computational complexity. On the other hand, conventional link adaptation technique could not perform well due to irregularities between the MCS levels which degraded the system throughput performance.

2) OUTAGE PROBABILITY PERFORMANCE CURVES

Furthermore, we compare the outage probability to validate the superiority of our proposed link adaptation algorithm. The outage probability equation is:

$$P(\text{outage}) = 1 - P(SINR > SINR\_Threshold) \quad (15)$$

where $P(SINR > SINR\_Threshold)$ is the probability when UE Rx SINR is higher than the SINR threshold, and then, UE is not considered to be in outage.

It can be clearly seen that from Fig. 13(b) that, outage probability decreased by using the proposed link adaptation technique. For example, if we compare the outage probability performance at 2 dB of SINR threshold then it can be easily observed that around 68 % receivers are in outage by using the proposed link adaptation technique. On the other, 82 % receivers are in outage when the conventional link adaptation technique is employed. Hence, the proposed link adaptation is performing well in the UAC system due to the benefit of less computational complexity as well as adapting the links smoothly.

VII. CONCLUSIONS

In this paper, we analyze an effective SNR mapping method and link adaptation approach using LLS and SLS via link 1 (an underwater base station controller to a UBS) for UAC network systems. To the best of our knowledge, this work is the first to take account of L2S mapping issues using a UAC network LLS to obtain abstraction for the development of a complete UAC network SLS. Moreover, for an accurate L2S mapping model, we calibrate and optimize the beta factors. Indeed, an effective SNR method for L2S mapping in a UAC network is performed based on the EESM method. The relationship between BLER and an effective SNR is mainly dependent on the MCS level used for transmitting data. BLER values are affected by the channel characteristics. BLER-versus-effective-SNR results are obtained for the desired beta values of BPSK, QPSK, and 16QAM in a

UAC network. Furthermore, we analyze the link adaptation strategy based on an adaptive modulation scheme using PF scheduling in the frequency domain, while time domain scheduling is performed based on RR UBS selection as well as PF-based UBS selection. In Fig. 12, the bold red and brown curves follow the adaptive modulation strategy, which shows the usefulness of link adaptation. In this paper, our main concern is to point out the effectiveness of the link adaptation approach by considering the practical environment of a UAC network. Unlike previous research on link adaptation optimization, up to now, we have focused on finding the suitability of the link adaptation procedure that can be compatible with the current specified receiver measurement, CQI feedback, and MCS selection and scheduling procedures. Our next target is to analyze the link adaptation strategy and underwater channel characteristics via UAC link 2 (UBS to sensor nodes) communications.

REFERENCES

[1] F. Qu, Z. Wang, L. Yang, and Z. Wu, "A journey toward modeling and resolving Doppler in underwater acoustic communications," *IEEE Commun. Mag.*, vol. 54, no. 2, pp. 49–55, Feb. 2016.

[2] M. Stojanovic and P. Beaujean, "Acoustic communication," in *Springer Handbook of Ocean Engineering*, M. R. Dhanak and N. I. Xiros, Ed. New York, NY, USA: Springer, 2016, pp. 359–383.

[3] T. Melodia, H. Kulhandjian, and E. Demirors, "Advances in underwater acoustic networking," in *Mobile Ad-Hoc Networking: Cutting Edge Directions*, 2nd ed. S. Basagni, M. Conti, S. Giordano, and I. Stojmenovic, Ed. Hoboken, NJ, USA: Wiley, 2013, pp. 504–854.

[4] M. Stojanovic and J. Preisig, "Underwater acoustic communication channels: Propagation models and statistical characterization," *IEEE Commun. Mag.*, vol. 47, no. 1, pp. 84–89, Jan. 2009.

[5] C. R. Berger, S. Zhou, J. C. Preisig, and P. Willett, "Sparse channel estimation for multicarrier underwater acoustic communication: From subspace methods to compressed sensing," *IEEE Trans. Signal Process.*, vol. 58, no. 3, pp. 1708–1721, Mar. 2010.

[6] S.-U. Kim, H.-S. Cheon, S.-B. Seo, S.-M. Song, and S.-Y. Park, "A hexagon tessellation approach for the transmission energy efficiency in underwater wireless sensor networks," *J. Inf. Process. Syst.*, vol. 6, no. 1, pp. 53–66, Mar. 2010.

[7] M. Stojanovic, "On the design of underwater acoustic cellular systems," in *Proc. OCEANS*, Aberdeen, U.K., Jun. 2007, pp. 1–6.

[8] B. Sirinivasan, "Capacity of underwater acoustic OFDM cellular networks," M.S. thesis, Dept. Comput. Sci. Eng., Univ. California, Santa Barbara, CA, USA, 2008.

[9] I. Ahmad, Z. Kaleem, and K. H. Chang, "Block error rate and UE throughput performance evaluation using LLS and SLS in 3GPP LTE downlink," in *Proc. Korean Inst. Commun. Inf. Sci.*, Daegwallyeong-myeon, South Korea: Yongpyong Resort, Feb. 2013, pp. 512–516.

[10] C. Mehlfuhrer, J. C. Ikuno, S. Šhwarz, S. Schwarz, M. Wrulich, and M. Rupp, "The Vienna LTE simulators—Enabling reproducibility in wireless communications research," *EURASIP J. Adv. Signal Process.*, vol. 2011, no. 29, pp. 1–14, Jan. 2011.

[11] C. Mehlführe, M. Wrulich, J. C. Ikuno, D. Bosanska, and M. Rupp, "Simulating the long term evolution physical layer," in *Proc. Eur. Signal Process. Conf.*, Glasgow, U.K., Aug. 2009, pp. 1471–1478.

[12] W. Chen, I. Ahmad, and K. Chang, "Co-channel interference management using eICIC/FeICIC with coordinated scheduling for the coexistence of PS-LTE and LTE-R networks," *EURASIP J. Wireless Commun.*, vol. 2017, p. 34, Dec. 2017. [Online]. Available: https://jwcn-eurasipjournals.springeropen.com/articles/10.1186/s13638-017-0822-6

[13] R. B. Santos, W. C. Freitas, Jr., E. M. Stancanelli, and F. R. Cavalcanti, "Link-to-system level interface solutions in multistate channels for 3gpp lte wireless system," in *Proc. Simposio Brasileiro Telecommun.*, São Pedro, Brazil, Dec. 2007, pp. 1–6.

[14] X. He, K. Niu, Z. He, and J. Lin, "Link layer abstraction in MIMO-OFDM system," in *Proc. IEEE Int. Workshop Cross Layer Design*, Sep. 2007, pp. 41–44.

[15] I. F. Akyildiz, D. Pompili, and T. Melodia, "Underwater acoustic sensor networks: Research challenges," *Ad Hoc Netw.*, vol. 5, no. 3, pp. 257–279, May 2005.

[16] R. Headrick and L. Freitag, "Growth of underwater communication technology in the U.S. Navy," *IEEE Commun. Mag.*, vol. 47, no. 1, pp. 80–82, Jan. 2009.

[17] N. Li, J.-F. Martínez, J. M. M. Chaus, and M. Eckert, "A survey on underwater acoustic sensor network routing protocols," *Sensors*, vol. 16, no. 3, p. 414, Mar. 2016.

[18] P. C. Etter, "*Underwater Acoustic Modeling and Simulation*, 4th ed. Boca Raton, FL, USA: CRC Press, 2013.

[19] Y. Noh *et al.*, "DOTS: A propagation delay-aware opportunistic MAC protocol for mobile underwater networks," *IEEE Trans. Mobile Comput.*, vol. 13, no. 4, pp. 766–782, Apr. 2014.

[20] T. Ebihara and K. Mizutani, "Underwater acoustic communication with an orthogonal signal division multiplexing scheme in doubly spread channels," *IEEE J. Ocean. Eng.*, vol. 39, no. 1, pp. 47–58, Jan. 2014.

[21] K. Chen, M. Ma, E. Cheng, F. Yuan, and W. Su, "A survey on MAC protocols for underwater wireless sensor networks," *IEEE Commun. Surv. Tuts.*, vol. 16, no. 3, pp. 1433–1447, Mar. 2014.

[22] M. Hayajneh, I. Khalil, and Y. Gadallah, "An OFDMA-based MAC protocol for under water acoustic wireless sensor networks," in *Proc. Int. Conf. Wireless Commun. Mobile Comput., Connecting World Wirelessly*, Leipzig, Germany, Jun. 2009, pp. 810–814.

[23] I. M. Khalil, Y. Gadallah, M. Hayajneh, and A. Khreishah, "An adaptive OFDMA-based MAC protocol for underwater acoustic wireless sensor networks," *Sensors*, vol. 12, no. 7, pp. 8782–8805, Jun. 2012.

[24] J.-W. Lee and H.-S. Cho, "Cascading multi-hop reservation and transmission in underwater acoustic sensor networks," *Sensors*, vol. 14, no. 10, pp. 18390–18409, Oct. 2014.

[25] H.-H. Ng, W.-S. Soh, and M. Motani, "MACA-U: A media access protocol for underwater acoustic networks," in *Proc. IEEE GLOBECOM*, New Orleans, LO, USA, Dec. 2008, pp. 1–5.

[26] P. Karn, "MACA-a new channel access method for packet radio," in *Proc. ARRL/CRRL Amateur Radio Comput. Netw. Conf.*, London, ON, Canada, Sep. 1990, pp. 134–140.

[27] J.-P. Kim, J.-W. Lee, Y.-S. Jang, K. Son, and H.-S. Cho, "A CDMA-based MAC protocol in tree-topology for underwater acoustic sensor networks," in *Proc. Int. Conf. Adv. Inf. Netw. Appl. Workshops*, Bradford, U.K., May 2009, pp. 1166–1171.

[28] D. Pompili, T. Melodia, and I. F. Akyildiz, "A CDMA-based medium access control for underwater acoustic sensor networks," *IEEE Trans. Wireless Commun.*, vol. 8, no. 4, pp. 1899–1909, Apr. 2009.

[29] P. Casari, B. Tomasi, and M. Zorzi, "A comparison between the Tone-Lohi and Slotted FAMA MAC protocols for underwater networks," in *Proc. IEEE OCEANS*, Quebec City, QC, Canada, Sep. 2008, pp. 1–8.

[30] R. Santos *et al.*, "Scheduling real-time traffic in underwater acoustic wireless sensor networks," in *Ubiquitous Computing and Ambient Intelligence*. Gran Canaria, Spain: Springer, Nov. 2016, pp. 150–162.

[31] H. Yan, Z. J. Shi, and J.-H. Cui, "DBR: Depth-based routing for underwater sensor networks," in *Proc. Int. Conf. Res. Netw.*, Singapore, vol. 86, May 2008, pp. 72.

[32] S. Gopi, G. Kannan, U. B. Desai, and S. N. Merchant, "Energy optimized path unaware layered routing protocol for underwater sensor networks," in *Proc. IEEE Global Telecommun.*, New Orleans, LO, USA, Dec. 2008, pp. 1–6.

[33] N. Z. Zenia, M. Aseeri, M. R. Ahmed, Z. I. Chowdhury, and M. S. Kaiser, "Energy-efficiency and reliability in MAC and routing protocols for underwater wireless sensor network: A survey," *J. Netw. Comput. Appl.*, vol. 71, pp. 72–85, Aug. 2016.

[34] X. Zhong, F. Chen, J. Fan, Q. Guan, F. Ji, and H. Yu, "Throughput analysis on 3-dimensional underwater acoustic network with one-hop mobile relay," *Sensors*, vol. 18, no. 2, p. 252, Jan. 2018.

[35] A. Khan *et al.*, "Routing protocols for underwater wireless sensor networks: Taxonomy, research challenges, routing strategies and future directions," *Sensors*, vol. 18, no. 5, p. 1619, May 2018.

[36] F. Ahmed, Z. Wadud, N. Javaid, N. Alrajeh, M. S, Alabed, and U. Qasim, "Mobile sinks assisted geographic and opportunistic routing based interference avoidance for underwater wireless sensor network," *Sensors*, vol. 18, no. 4, p. 1062, Apr. 2018.

[37] T. S. Rappaport, *Wireless Communications: Principles and Practice*, 2nd ed. Upper Saddle River, NJ, USA: Prentice-Hall, 1996, p. 736.

[38] I. Ahmad, Z. Kaleem, and K. H. Chang, "Uplink power control for interference mitigation based on users priority in two-tier femtocell network," in *Proc. IEEE Int. Conf. ICT Converg.*, Jeju, Korea, Oct. 2013, pp. 474–475.
[39] I. Ahmad, W. Chen, and K. H. Chang, "Co-channel interference analysis using cooperative communication schemes for the coexistence of PS-LTE and LTE-R networks," in *Proc. IEEE Commun. Electron. Special Session LTE Technol. Services*, Hanoi, Vietnam, Jul. 2016, pp. 181–182.
[40] I. Ahmad, W. Chen, and K. H. Chang, "LTE-railway user priority-based cooperative resource allocation schemes for coexisting public safety and railway networks," *IEEE Access*, vol. 5, pp. 7958–8000, May 2017.
[41] Z. Kaleem, Y. Li, and K. H. Chang, "Public safety users" priority-based energy and time-efficient device discovery scheme with contention resolution for ProSe in third generation partnership project long-term evolution-advanced systems," *IET Commun.*, vol. 10, no. 15, pp. 1873–1883, 2016.
[42] M. Stojanovic, "Design and capacity analysis of cellular-type underwater acoustic networks," *IEEE J. Ocean. Eng.*, vol. 33, no. 2, pp. 171–181, Apr. 2008.
[43] A. Radosevic, T. M. Duman, J. G. Proakis, and M. Stojanovic, "Channel prediction for adaptive Modulation in underwater acoustic communications," in *Proc. IEEE OCEANS*, Santander, Spain, Jun. 2011, pp. 1–5.
[44] M. Stojanovic, "On the relationship between capacity and distance in an underwater acoustic communication channel," in *Proc. Int. Conf. Under-Water Netw. Syst.*, Los Angeles, CA, USA, Sep. 2006, pp. 41–47.
[45] A. Stefanov and M. Stojanovic, "Clustered underwater ad-hoc networks in the presence of interference," in *Proc. IEEE Asilomar Conf. Signals, Syst. Comput.*, Pacific Grove, CA, USA, Nov. 2010, pp. 1908–1912.
[46] R. Cao, L. Yang, and F. Qu, "On the capacity and system design of relay-aided underwater acoustic communications," in *Proc. IEEE Wireless Commun. Netw. Conf.*, Sydney, NSW, Australia, Apr. 2010, pp. 1–6.
[47] A. Stefanov and M. Stojanovic, "Design and performance analysis of underwater acoustic networks," *IEEE J. Sel. Areas Commun.*, vol. 29, no. 10, pp. 2012–2021, Dec. 2011.
[48] K. Stamatiou, P. Casari, and M. Zorzi, "The throughput of underwater networks: Analysis and validation using a ray tracing simulator," *IEEE Trans. Wireless Commun.*, vol. 12, no. 3, pp. 1108–1117, Mar. 2013.
[49] I. F. Akyildiz, P. Wang, and S.-C. Lin, "SoftWater: Software-defined networking for next-generation underwater communication systems," *Ad Hoc Netw.*, vol. 46, pp. 1–11, Aug. 2016.
[50] K. G. Kebkal and R. Bannasch, "Sweep-spread carrier for underwater communication over acoustic channels with strong multipath propagation," *J. Acoustic Soc. Amer.*, vol. 112, pp. 2043–2052, Nov. 2002.
[51] L. Wan *et al.*, "Adaptive modulation and coding for underwater acoustic OFDM," *IEEE J. Ocean. Eng.*, vol. 40, no. 2, pp. 327–336, Apr. 2015.
[52] E. Demirors, G. Sklivanitis, T. Melodia, G. E. Santagati, and S. N. Batalama, "A high-rate software-defined underwater acoustic modem with real-time adaptation capabilities," *IEEE Access*, vol. 6, pp. 18602–18615, Apr. 2018.
[53] L. M. Brekhovskikh and Y. P. Lysanov, *Fundamental of Ocean Acoustics*, 3rd ed. New York, NY, USA: Springer, 1982.
[54] *System-level Evaluation of OFDM—Further Considerations*, document 3GPP TSG-RAN-1. R1-031303, Portugal, 2003.
[55] K.-B. Song, A. Ekbal, S. T. Chung, and J. M. Cioffi, "Adaptive modulation and coding (AMC) for bit-interleaved coded OFDM (BIC-OFDM)," *IEEE Trans. Wireless Commun.*, vol. 5, no. 7, pp. 1685–1694, Jul. 2006.
[56] J. M. Cioffi, "EE379C-Digital communication: Signal processing," Stanford Univ., Stanford, CA, USA, Tech. Rep., 2008. [Online]. Available: https://web.stanford.edu/class/ee379c/reader.html
[57] C. K. Sung, S.-Y. Chung, J. Heo, and I. Lee, "Adaptive bit-interleaved coded OFDM with reduced feedback information," *IEEE Trans. Wireless Commun.*, vol. 55, no. 9, pp. 1649–1655, Sep. 2007.
[58] M. Sadeghi, M. Elamassie, and M. Uysal, "Adaptive OFDM-based acoustic underwater transmission: System design and experimental verification" in *Proc. IEEE Int. Black Sea Conf. Commun. Netw.*, Istanbul, Turkey, Jun. 2017, pp. 1–5.

ISHTIAQ AHMAD received the B.S. degree in electrical engineering from the University of Engineering and Technology (UET), Peshawar, Pakistan, in 2007, and the M.S. degree in electronic engineering from Inha University, South Korea, in 2014, where he is currently pursuing the Ph.D. degree with the Electronic Engineering Department.

From 2007 to 2008, he was a BSS Engineer with O&M Department, Zong Pakistan. Since 2009, he has been a Lecturer with the Faculty of Engineering and Technology, Gomal University, Pakistan. He has authored several international journals and IEEE conference papers, and also holds US and Korean patents. His research interests include interference management in 3GPP LTE-A & 5G systems, cross-layer design, public safety & mobile ad-hoc networks (for AUV & Ship), maritime/underwater communications, and connected-autonomous vehicle (C-AV).

Mr. Ahmad was a recipient of the Jungseok International Scholarship to pursue his M.S. and Ph.D. degrees at Inha University, due to his excellent academic career. He received the Outstanding Research Award from the Inha University, in 2019, for his Excellence of Journal Publication.

KYUNGHI CHANG (SM'98) received the B.S. and M.S. degrees in electronics engineering from Yonsei University, Seoul, South Korea, in 1985 and 1987, respectively, and the Ph.D. degree in electrical engineering from Texas A&M University, College Station, TX, USA, in 1992. From 1989 to 1990, he was with the Samsung Advanced Institute of Technology (SAIT) as a member of the research staff and was involved in digital signal processing system design. From 1992 to 2003, he was with the Electronics and Telecommunications Research Institute (ETRI) as a Principal Member of the technical staff, where he led the design teams involved in the WCDMA UE modem and 4G radio transmission technology (RTT). He is currently with the Electronic Engineering Department, Inha University. His research interests include 3GPP LTE-A & 5G New RAT, HetNet, cross-layer design, public safety and mobile ad-hoc networks (for AUV & Ship), maritime/underwater communications, and connected-autonomous vehicle (C-AV). He was a recipient of the LG Academic Awards, in 2006, the Haedong Best Paper Awards, in 2007, the IEEE ComSoc Best Paper Awards, in 2008, the Haedong Academic Awards, in 2010, and the SKT SafeNet Best Idea Awards, in 2015. He is currently a Chairman of the expert committee in SafeNet Forum, and mobile and automotive convergence committee in 5G Forum. He has served as an Editor-in-Chief and an Executive Director for the *Journal of Korean Institute of Communications and Information Sciences* (KICS), from 2010 to 2012 and in 2013, respectively. He has also served as an Editor of ITU-R TG8/1 IMT.MOD.